CONTRAST MEDIA & MOLECULAR IMAGING

Received: 16 June 2013, Revised: 20 September 2013, Accepted: 26 October 2013, Published online in Wiley Online Library

(wileyonlinelibrary.com) DOI: 10.1002/cmmi.1582

In vivo MRI mapping of iron oxide-labeled stem cells transplanted in the heart

A. Ruggiero[a]*†, J. Guenoun[a†], H. Smit[b], G. N. Doeswijk[a], S. Klein[b], G. P. Krestin[a], G. Kotek[a] and M. R. Bernsen[a,c]

In various stem cell therapy approaches poor cell survival has been recognized as an important factor limiting therapeutic efficacy. Therefore noninvasive monitoring of cell fate is warranted for developing clinically effective stem cell therapy. In this study we investigated the use of voxel-based R_2 mapping as a tool to monitor the fate of iron oxide-labeled cells in the myocardium. Mesenchymal stem cells were transduced with the luciferase gene, labeled with ferumoxide particles and injected in the myocardium of healthy rats. Cell fate was monitored over a period of 8 weeks by bioluminescence and quantitative magnetic resonance imaging. Bioluminescence signal increased during the first week followed by a steep decrease to undetectable levels during the second week. MR imaging showed a sharp increase in R_2 values shortly after injection at the injection site, followed by a very gradual decrease of R_2 over a period of 8 weeks. No difference in the appearances on R_2-weighted images was observed between living and dead cells over the entire time period studied. No significant correlation between the bioluminescence optical data and R_2 values was observed and quantitative R_2 mapping appeared not suitable for the *in vivo* assessment of stem cell. These results do not follow previous *in vitro* reports where it was proposed that living cells may be distinguished from dead cells on the basis of the R_2 relaxivities (intracellular and extracellular iron oxides). Cell proliferation, cell migration, cell death, extracellular superparamagnetic iron oxide dispersion and aggregation exhibit different relaxivities. *In vivo* these processes happen simultaneously, making quantification very complex, if not impossible. Copyright © 2013 John Wiley & Sons, Ltd.

Keywords: Magnetic resonance imaging; stem cell tracking; R2 Mapping

1. INTRODUCTION

Regenerative approaches in the treatment of myocardial infarction have been widely investigated in the past few years, fueling new hopes for patients and scientists. Preclinical evidence that stem-cell-based therapy has the potential to limit the degradation of cardiac function after myocardial infarction led to the rapid development of several clinical trials (1). Recent meta-analyses reported a modest but statistically significant improvement in the ejection fraction, ventricular dimension and infarct area (2,3). One or more imaging techniques were greatly exploited in these clinical trials; however, only indirect indications of the efficacy of stem cell transplantation was provided by the evaluation of myocardial contractility, viability and perfusion. While these results depict a promising picture of the stem cell-based therapy, questions have been raised regarding actual grafting, transformation and proliferation of stem cells in the host tissue (and therefore recovery of the physiological functions of the organ) or whether or not the transplanted cells simply exert paracrine effects (which can induce the recovery of the host tissue) (4).

Molecular imaging (MI) techniques allow the direct visualization of stem cells, their short- and long-term fate and eventually their viability (5). Cell labeling approaches for these purposes include generally reporter genes or chemical-based contrast agents (5). The former requires the introduction of a reporter gene into the cells of interest, through viral or nonviral-vectors. The reporter gene encodes for a protein (enzymes, receptor, transporter) able to interact with a correspondent reporter probe which is activated or concentrated only in the cells expressing the reporter gene. Probe accumulation is proportional to the expression level of the reporter gene; therefore, the number of living cells or the induction of a specific reporter gene can be quantified. Passive loading of cells with radioactive agents (^{18}F-FDG, ^{111}In-Oxine, etc.) for positron emission tomography (PET)/single photon emission or contrast agents (iron oxides, gadolinium, manganese, ^{19}F) for magnetic resonance imaging (MRI) is another approach commonly used for cell tracking (5,6).

Labeling with superparamagnetic iron oxide (SPIO) nanoparticles has been extensively studied as they act as magnetic inhomogeneities, locally disturbing the magnetic field, inducing a significant increase of R_2- and R_2*-relaxation rates (hypointense signal). Studies reported that SPIOs do not affect cell viability, proliferation, differentiation or migration (7–10). However, a major drawback is

* *Correspondence to: A. Ruggiero, Department of Radiology, Erasmus MC, Rotterdam, The Netherlands. E-mail: al.ruggiero@gmail.com*

† *The first two authors contributed equally.*

a *A. Ruggiero, J. Guenoun, G. N. Doeswijk, G. P. Krestin, G. Kotek, M. R. Bernsen*
Department of Radiology, Erasmus MC, Rotterdam, The Netherlands

b *H. Smit, S. Klein*
Biomedical Imaging Group Rotterdam, Departments of Medical Informatics and Radiology, Erasmus MC, Rotterdam, The Netherlands

c *M. R. Bernsen*
Department of Nuclear Medicine, Erasmus MC, Rotterdam, The Netherlands

related to the persistence of the hypointense signal at the site of transplant regardless of labeled cell viability. In fact, at longer time points SPIO-induced signal loss is not necessarily associated with implanted cells but rather with phagocytosing monocytes (11,12). Intriguingly, SPIO induced relaxivities have been shown to be dependent on their location; that is, the relaxivities are different when SPIOs are compartmentalized within the intracellular space or dispersed in the extracellular space (13,14). Indeed, increased R_2 values have been reported in lysed vs viable SPIO-labeled cells, this effect is related to limited SPIO-proton interaction in the intracellular compartment compared with unlimited proton interactions of SPIO released from disrupted cells (15,16).

The majority of cell tracking studies in the heart have focused on the potential of SPIO labeling and MRI longitudinal follow-up of implanted cells, relying on a semi-quantitative approach based on signal intensity (signal-to-noise measurements). A quantitative approach has already been used for the evaluation of SPIO-labeled cells *in vivo* (17), but it has never been exploited to assess SPIO-labeled cells implanted in the heart. In this work, we aimed: (a) to perform quantitative R_2 mapping of the heart at 7 T; (b) to assess reproducibility and robustness of the technique; and (c) to assess longitudinally *in vivo* the R_2 changes related to cell proliferation and cell death as evaluated by bioluminescence of double-labeled rat mesenchymal stem cells (rMSCs).

2. RESULTS AND DISCUSSION

2.1. Viability Assessment

Analysis of iron content by inductively coupled plasma optical emission spectroscopy measurements revealed 7.58 ± 0.09 iron pg/cell (rMSC) and 7.67 ± 0.14 iron pg/cell (rMSC-Fluc) after the labeling procedure. The difference was not statistically significant. In order to assess whether the cell manipulation (Fluc transduction) or cell labeling could affect cell viability, cell proliferation studies were performed (Fig. 1). The presence of the Fluc gene in these cells reduced proliferation rate compared with the wild type as lower cell counts were observed in the rMSC-Fluc compared with the rMSC at all time points ($p < 0.05$).

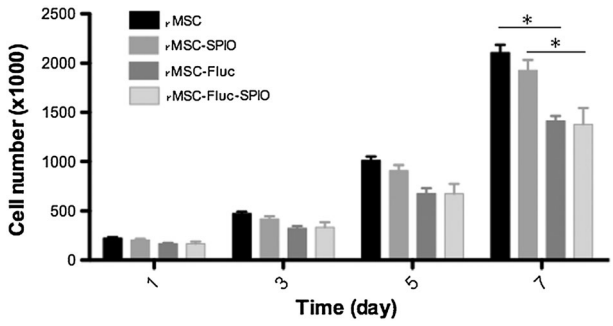

Figure 1. Effect of cell labeling on growth profile. Rat mesenchymal stem cells (rMSCs) and rMSC-Fluc were labeled with superparamagnetic iron oxide (SPIO), cultured for 7 days and cells were counted at different time points. A lower cell count was observed in the rMSC-Fluc (doubling time, 2.02 days) compared with the rMSC (doubling time, 1.85 days) at all time points ($p < 0.05$). A lower cell count was observed with rMSC-SPIO labeled cells compared with control cells (rMSC) only on day 7 ($p < 0.05$). SPIO labeling of rMSC-Fluc cell did not have any statistically significant effect on cell proliferation compared with unlabeled control.

Lower cell counts were observed with rMSC-SPIO labeled cells compared with control cells only on day 7 ($p < 0.05$). SPIO labeling of rMSC-Fluc cells did not have any statistically significant effect on cell proliferation compared with unlabeled rMSC-Fluc control. Doubling times (expressed in days) were calculated to be: 1.85 (rMSC unlabeled), 1.86 (rMSC labeled with SPIO), 2.02 (rMSC-Fluc unlabeled) and 2.05 (rMSC-Fluc labeled with SPIO). Doubling time of rMSC-Fluc was statistically different from rMSC at all time points ($p < 0.05$).

2.2. Reproducibility Study

Using a black blood fast spin echo (BBFSE)-based mapping approach, the robustness of the R_2 ($1/T_2$) value measurements was assessed (18). Figure 2 shows a representative axial slice of a healthy rat heart (no injection). The measured points show a clear exponential signal decay and calculated errors were relatively small. The signal was quite homogenous with T_2 values (22.47 ± 1.92 ms) in the preferred area for cell injection (anterior and anterolateral segment). However, some regions such as the septal and the inferolateral region were more prone to movement artifacts (e.g. breathing) and were associated with a less reliable curve fitting.

Reproducibility studies were performed in four animals scanned four times each to assess the robustness of the technique (Fig. 3). Regarding repeated measures of R_2 in subsequent imaging sessions, the following variability was observed: region 1, 21.72 ± 1.49 ms; region 2, 22.68 ± 1.7 ms; region 3, 26.17 ± 2.13 ms; region 4, 22.62 ± 1.68 ms; region 5, 25.99 ± 2.49 ms; region 6, 21.54 ± 1.86 ms (Fig. 3). All intraclass correlation coefficients, as a measure of the reliability of measurements, varied between 0.75 and 0.80, which is considered 'acceptable reliability'. One-way ANOVA was used to test spatial variability of R_2 and T_2 values of the six different heart segments

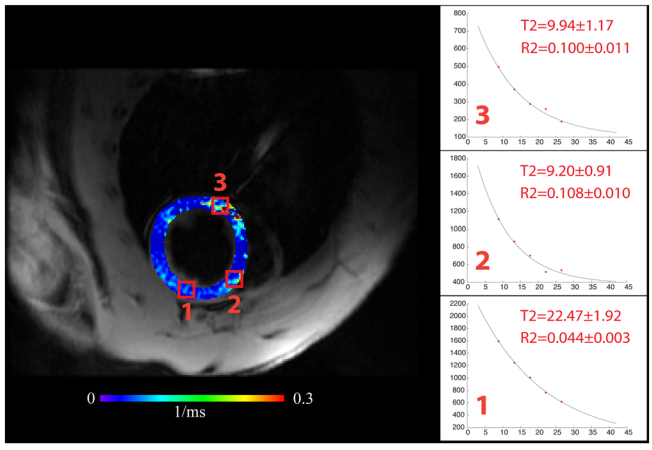

Figure 2. R_2 value variability in healthy heart. Representative image depicting an axial slice of a healthy rat heart with superimposed R_2 values measured by using a black blood fast spin echo (BBFSE) based mapping approach. The exponential curve of the average signal decay is shown for the three regions and calculated T_2 and R_2 (mean ± square root of the Cramer–Rao lower bounds) are reported. The signal is quite homogenous in the area corresponding to the preferred cell injection site in this study (anterior and anterolateral segment). However some regions such as the septal region and the inferolateral region are affected by movement artifacts (breathing, blood flow) and are associated with unreliable curve fitting.

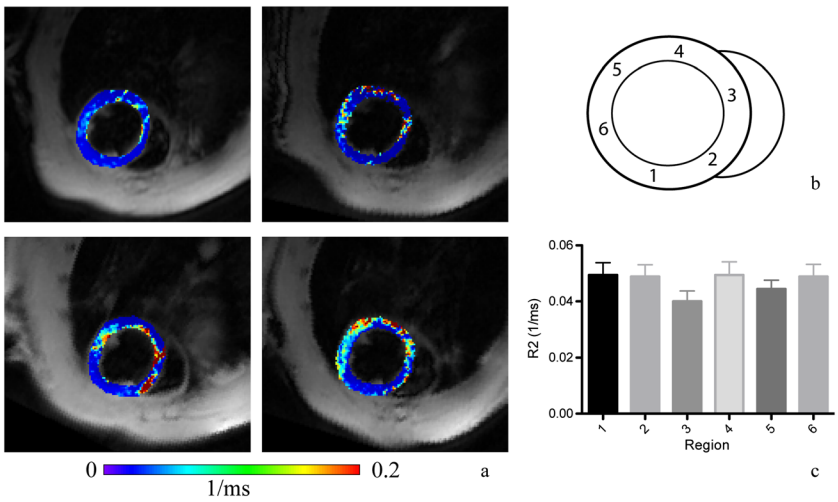

Figure 3. Reproducibility study. (a) A representative BBFSE image with superimposed R_2 mapping values, of an animal imaged in four separate sessions. (b) Schematic drawing of the region distribution. Region 1, anterior; region 2, antero-septal; region 3, inferoseptal; region 4, inferior; region 5, inferolateral; region 6, anterolateral. (c) The variability of R_2 values (mean ± standard error of the mean, SEM) observed in the different heart regions of four animals in four different imaging sessions.

of four animals. We did not observe a statistically significant difference among the different segments ($p > 0.05$).

2.3. Imaging Cell Fate

The viability and proliferation of implanted cells were assessed longitudinally *in vivo* in group 1 ($n = 9$), by both bioluminescence imaging and MR imaging. We observed an increase in optical signal over days 3–7 (compared with day 3, a 3-fold and 15-fold increase at days 5 and 7, respectively) upon injection of viable cells, most probably related to cell proliferation in the implantation site. On day 10 the signal had declined substantially (0.7-fold reduction compared with highest peak at day 7) and reached background levels on day 15.

In MR images, large areas of hypointensity, generated by iron-labeled cells, were clearly visible in the MRI scans of the injected hearts. Importantly, no difference was observed in terms of size, number and distribution of these signal voids between living and nonviable cells. Longitudinal MRI scans were performed to assess the changes in R_2 relaxivity over time, related to SPIO dilution or potential decompartmentalization upon cell proliferation or cell death, respectively. Quantification of the signal revealed a 2-fold significant increase ($p < 0.05$) in R_2 between days 3 and 5 after injection (Fig. 4). This was probably related to the early reabsorption of the injection volume with redistribution of the cells in the implantation site. From day 5 onwards, R_2 values decreased. In sham injected animals (group 3, $n = 3$), no changes in the R_2 values over time were observed at the site of the presumed injection. No statistical correlation with the proliferation or viability profile monitored by bioluminescence was observed ($p = 0.1$). We investigated whether the relaxivity changes associated with the decompartmentalization of iron oxides might be quantified by MRI. We injected a solution of SPIO-labeled rMSC-Fluc that was no longer viable (as an effect of repeated freeze/thawing cycles and brief sonication), therefore containing the same amount of SPIO as the viable cells but dispersed in the extracellular compartment. No difference was observed in terms of size, number and distribution of the generated signal voids between living and nonviable cells on T_2-weighted images. Higher R_2 values were associated with dead compared with the viable ones, however the difference was statistically significant only on day 3. The dead cells showed a similar trend to viable cells, consisting in an increase in R_2 on day 5 followed by a decrease.

Histological analysis of cryo-sections of hearts revealed that injections with nonviable SPIO-labeled cells were associated with a more punctate appearance of the iron stain (owing to the extracellular release of SPIO in the injection solution). Conversely the iron staining of viable SPIO-labeled cells depicted larger aggregates (Fig. 6).

3. DISCUSSION

The ability to monitor the localization, viability, proliferation and possibly the differentiation status of implanted stem cells provides massive benefit in regenerative medicine approaches. All of the pre-clinical and clinical imaging techniques have been leveraged towards this goal, each providing unique advantages and limitations (5). MRI is a widely established technique for the evaluation of cardiac anatomy and function. Taking advantage of its excellent spatial resolution [10–100 μm (preclinical); 500–1500 μm (clinical)], stem cells labeled with superparamagnetic and paramagnetic agents can be visualized (19,20). The choice of a proper labeling marker is, however, a crucial aspect of cell tracking by MRI. High sensitivity allows the long-term evaluation of implanted stem cells, since probe dilution upon cell proliferation reduces the detection capabilities. Also, high specificity is demanded to investigate potential cell graft rejection at an early stage.

In this study, luciferase-expressing rMSC labeled with SPIO were implanted in the heart and longitudinally monitored by quantitative MRI (R_2 voxel based) and bioluminescence imaging. A vast amount of work has been performed on longitudinal imaging of implanted cells in the heart by MRI, SPIO-labeling and assessment of cell fate by means of (loss of) signal intensities on T_2-weighted images being the most used approach. The detection of low signal intensity

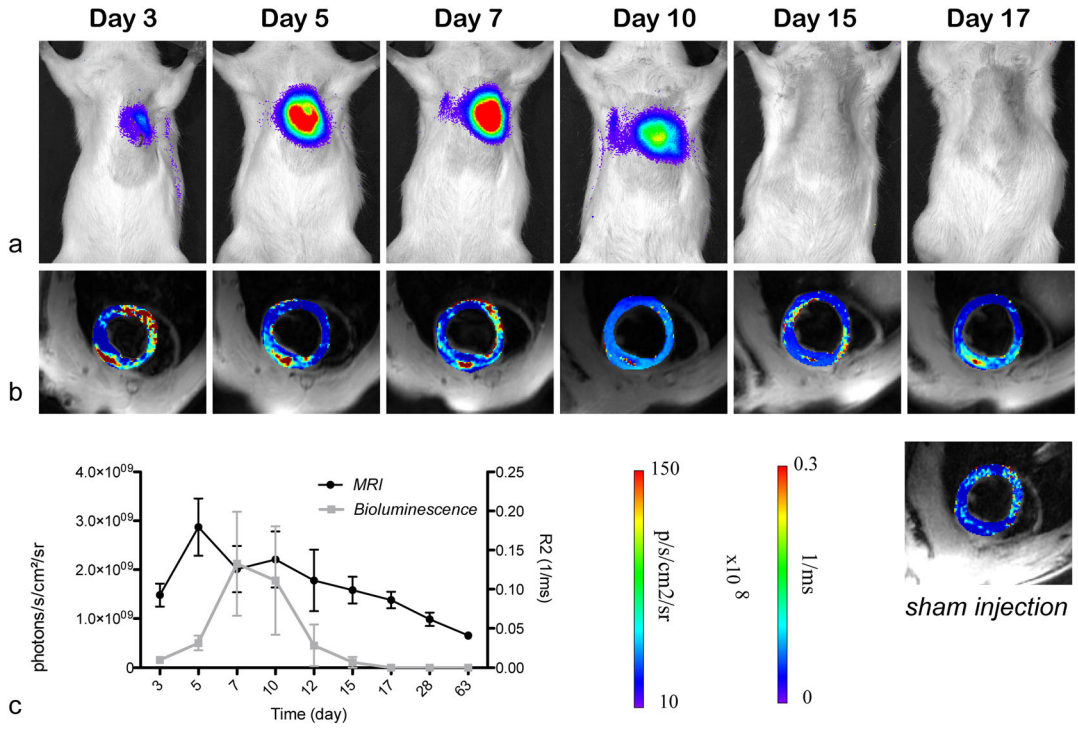

Figure 4. Longitudinal imaging of cell fate by bioluminescence and MRI. (a) Representative images showing the evolution over time of bioluminescent signal (according to the color-scale provided) emitted by intramyocardially injected rMSC-Luc-SPIO cells. (b) Representative images showing evolution of R_2 values (according to the color-scale provided) superimposed on a BBFSE image of a short axis slice of a rat heart at the level of injection with rMSC-Luc-SPIO cells. Bottom right image represents data observed in sham-operated animals.(c) Graph showing evolution of bioluminescent signal values and R_2 values of rat hearts ($n = 9$ at day 3; $n = 8$ at days 5–15; $n = 4$ at days 17–28; $n = 2$ at day 63) following intramyocardial injection of rMSC-Luc-SPIO cells (mean ± SEM).

areas is an insufficient method as it is associated with some limitations such as: (a) inhomogeneity in the coil sensitivity (phased-array coils determine regional myocardial signal variations that may give an inaccurate interpretation); (b) artifacts owing to motion and flow; and (c) the inherent qualitative aspect of this approach, whose evaluation relies on regional differences in signal intensity, which strongly depend on the parameters of the sequences used [repetition time (*TR*), echo time (*TE*), slice thickness, etc.] (21).

To overcome these limitations, the alternative approach consists of the direct quantification of the T_2 values of the myocardium. This allows the detection of subtle T_2 differences in tissues, reducing the subjective interpretation of signal voids (and their dependence from parameters) and minimizing flow or motion dependent artifacts (21). Many *in vivo* studies on T_2 mapping of the heart have been performed in humans in the last two decades, mainly based on spin echo acquisitions. Novel approaches based on T_2 prepared steady-state free precession (21), hybrid sequences (22), bright blood approaches (23) and additional adiabatic prepulses (24) have also been suggested recently. It is an area of active investigation for quantitative assessment of myocardial edema and iron overload. However, the use of quantitative mapping for quantification of SPIO-labeled cells implanted in the heart has been quite limited.

A few studies suggested R_2 ($1/T_2$) and R_2^* ($1/T_2^*$) parametric mapping as a reliable and reproducible quantification method of SPIO or SPIO-labeled cells per voxel (14,25,26). Importantly, variation of R_2 and R_2^* according to SPIO compartmentalization has been described. Phantom studies demonstrated that, with identical iron concentrations, cell-bound SPIO show higher R_2^* values compared with free SPIO. Conversely, R_2 measurements are higher for free iron than for intracellular iron (13,14).

We sought to use R_2 mapping as a means to detect, *in vivo*, changes associated with probe dilution and potential decompartmentalization of SPIO as a result of cell proliferation and cell death, respectively. We employed a double inversion recovery BBFSE sequence and tested its robustness in a reproducibility experiment. The signal was quite homogenous in the preferred regions for cell injection in these experiments such as the anterior and anterolateral segments with T_2 values of 22.47 ± 1.92 and 21.54 ± 1.86 ms (prior to injection), respectively (Figs 2 and 3). As expected, regions associated with higher cardiac motion (such as the septal and the inferolateral segment) corresponded on R_2 maps to unreliable curve fitting, as previously demonstrated (27). However, this limitation did not interfere with the longitudinal assessment of the relaxivity of the injected cells. Overall, the difference in R_2 and T_2 values among the six different segments was not statistically significant.

In the longitudinal assessment of implanted cells, bioluminescence showed an initial increase in the optical signal (peak on day 7), most probably related to cell proliferation, followed by a decrease in signal strength. Limited persistence of bioluminescent signal has been observed previously (28) and the explanation of the signal decrease is not univocal. Cell manipulation impairs cell proliferative ability (Fig. 1) and may induce further phenotypical changes that may lead to an immunogenic response by the host. Chen *et al.* reported, from *in vivo* studies with bioluminescence, a half-life of Fluc-labeled cells of 2.65 days, with an optical signal showing an increase within the first 3 days and further decrease with background levels on day

6. Our observations are in agreement with these and other findings, in which the majority (more than 70%) of cells implanted in the heart were reported to die within the first week of injection in immunocompetent animals (28–30). The decreasing signal might also result from epigenetic silencing of reporter gene expression, which complicates the overall quantification (31). This phenomenon does not seem likely in our study, since identically generated rMSC-Luc-SPIO cells were also injected in other anatomical locations in rats within our group, without a corresponding rapid loss of bioluminescent signal (32). The specific location of the cell implantation (e.g. beating heart vs skeletal muscle) might be also considered as a factor influencing the cell survival.

MRI has been used in *in vitro* studies to monitor cell proliferation; we and others previously reported that, under *in vitro* conditions, cell proliferation/division is associated with an R_2 decrease (13,16). Instead, when cells die, they spread their content to the extracellular matrix, determining a R_2 increase; this effect has been investigated only in *in vitro and ex vivo* studies. Simon *et al*. reported a statistically significant difference in R_2 relaxation times between viable and nonviable lysed cells (15). Similarly, Nedopil *et al*. investigated ferumoxide-labeled human mesenchymal stem cells implanted in *ex vivo* joints and showed on T_2-weighted images a markedly lower signal (thus shorter T_2) of apoptotic compared with viable cells (33). To our knowledge, this is the first attempt to investigate the quantitative approach of SPIO-labeled cell fate in an *in vivo* setting. We observed a 2-fold significant R_2 increase from days 3 to 5 after injection, which corresponded to the increasing optical bioluminescence signal (suggesting cell proliferation) (Fig. 4). From day 5 onwards, R_2 values started to decrease, whilst bioluminescence data continued to suggest ongoing proliferation. Overall we found no significant correlation between bioluminescent signal profiles and MRI signal evolution ($p = 0.1$). Moreover, we mimicked the release of SPIO content in the injection solution by inducing the death of SPIO-labeled rMSC before implantation in the heart. As expected, higher R_2 values were associated with the injection of nonviable vs viable cells. However, the difference was statistically significant only on day 3 (Figs 5 and 6).

We argued that the processes happening *in vivo* (such as cell redistribution in the injection site or the re-absorption of the injection medium with further changes in the interactions of the SPIO particles) might obscure the detection of potential changes associated with probe dilution and cell death, making the overall quantitative assessment complicated.

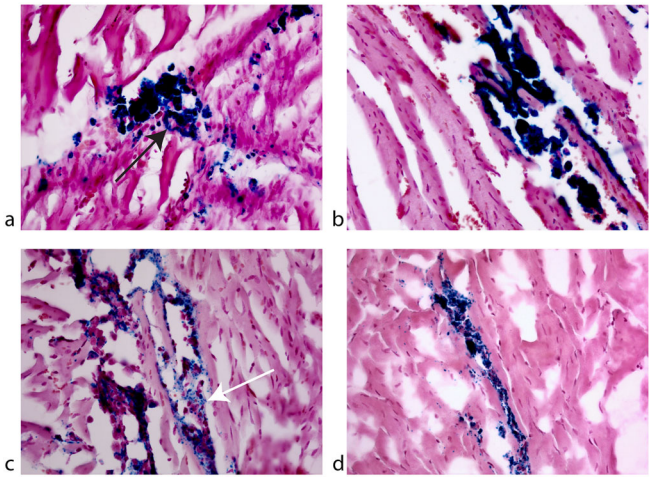

Figure 6. Representative histological sections of rat hearts injected with viable (upper panel) and nonviable (lower panel) SPIO-labeled cells harvested at 3 days (a, c) and 15 days (b, d) after injection. Iron staining (blue) depicts the presence of iron which is associated with larger aggregates in the viable cells (black arrow) compared with nonviable cells, which present a more punctate appearance (white arrow) owing to extracellular release of SPIO in the injection solution.

In addition to the above-mentioned physiological processes, endogenous cells (e.g. macrophages) might be involved in the potential re-uptake of the SPIO released in the extracellular matrix or phagocytosis of dead cells may intervene hampering the detection of the difference in the later days. Chen *et al*. reported a change in the histological pattern of ferumoxides injected in the myocardium, from dispersed (day 2) to focal (day 9), suggesting the involvement of macrophages in scavenging and concentrating SPIO (28). This is a common issue in the use of SPIO as a labeling marker, Winter *et al*. reported (by means of hypointensity) the absence of any discrimination between healthy successfully engrafted and dead SPIO labeled cells phagocytosed by macrophages within the heart. In particular,

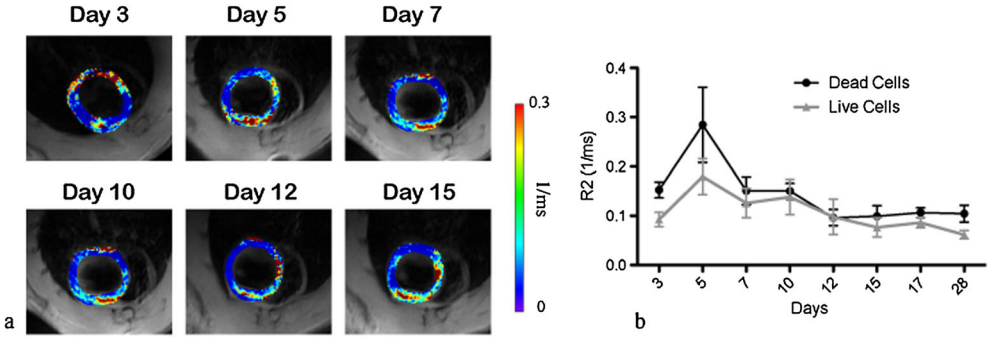

Figure 5. R_2 MRI mapping in viable and nonviable cells. (a) Representative images showing evolution of R_2 values superimposed on a BBFSE image of a short axis slice of a rat heart at the level of injection with nonviable rMSC-Luc-SPIO cells intramyocardially, over time according to the colorscale provided. (b) Graph showing evolution of R_2 values of rat hearts at the site of injection of living and dead rMSC-Luc-SPIO cells. SPIO labeled MSC-Fluc no longer viable (as an effect of repeated freeze/thawing cycles and brief sonication), containing the same amount of iron of viable cells but decompartmentalized were injected in the heart. As an effect of decompartmentalization of SPIO, nonviable cells are associated with higher R_2 values compared with viable cells, which is statistically significant different only at day 3 after cell implantation. The absence of a statistically significant difference in the remaining days is probably associated with the changes related to free SPIO in the extracellular matrix (such as the possible uptake from endogenous cells).

no differences in signal voids up to more than 40 days were observed between dead and viable cells recipients with respect to size, number and localization. Therefore, just signal loss in T_2-weighted MR images overestimates SPIO-labeled stem cells survival after transplantation in the heart (12). Similarly, by performing quantitative MRI mapping we were able to depict a slow decrease of the R_2 values of the injected cells, which remained higher than the relaxivity values of the normal myocardium for the length of our investigation. These findings confirmed for the first time by MRI mapping that SPIO is not a suitable probe for the longitudinal follow-up of the *in vivo* fate of implanted cells.

It is worth observing that one limitation of this study was related to a quantitative MRI approach based only on R_2 and not also R_2* measurements. First, because R_2* values are more sensitive to changes from the intracellular to the extracellular space (decrease) and second because a calculated R_2' ($R_2^* - R_2$) would probably have been more sensitive in depicting subtle changes. R_2* measurements have been attempted; however, we found this approach not possible to achieve at 7 T, since the R_2*-weighted MR signal disappears in a very short time, making impractical R_2* curve fitting with the current setup. Ultra short echo times should be employed to perform a proper R_2* mapping.

In conclusion, many of the techniques to image stem cells are promising but further work is required before a wide clinical translation becomes reality. From the review of the current literature it seems that there is 'no single best method', rather an array of different techniques, each one with specific advantages in terms of spatial resolution, sensitivity and specificity. Reporter gene imaging, considered as the most reliable approach in the quantitative short and long-term evaluation of engraftment and survival, is still associated with unsolved issues such as gene silencing, immunogenicity and debated safety. MRI offers great spatial resolution and quantitative capabilities; however currently available probes are sub-optimal. The development of hybrid techniques (MRI/PET) together with improved reporter genes would certainly play a role in the quantitative assessment of cell transplantation in longitudinal studies.

4. CONCLUSIONS

Cell proliferation, cell migration, cell death, extracellular SPIO dispersion or aggregation exhibit different relaxivities. No correlation between bioluminescence and R_2 mapping was observed in our experiments, showing conclusively that quantitative R_2 mapping is not suitable for the assessment *in vivo* of stem cells in the heart. Unless there is only one well-defined process happening in a restricted volume of interest, *in vivo* quantification is very complex, as previously demonstrated in *vitro* (13).

5. EXPERIMENTAL

5.1. Rat Mesenchymal Stem cells Expressing Firefly Luciferase

The plasmid pND-Cag-Fluc was co-transfected into 293 T cells with a mixture of Endofree Maxi-kit (Quiagen, Hilden Germany), VSVG (45 μg/dish), pMD and pRev using polyethylenimine (Sigma Aldrich, St Louis, MO, USA). Lentivirus supernatant was collected at 48 and 72 h, filtered (0.45 μm) and concentrated by sediment centrifugation. The pellet was then resuspended in 1 ml phospate buffered saline (PBS). Rat mesenchymal stem cells (Millipore, Billerica, MA, USA) were grown to 50% confluency in a 24 well plate in Dulbecco's modified Eagle medium (DMEM) /F10 (Invitrogen; Carlsbad, CA, USA), 10% fetal calf serum and infected with 50 μl lenti-viral stock. Viral titer was assessed on concentrated supernatant by HIV-p24 ELISA (Dupont, Wilmington, DE, USA). Transduced rMSC (rMSC-Fluc) were expanded and plated at low densities. The expression of Fluc was evaluated using a luminometer and clones with the highest expression of Fluc were selected and expanded.

5.2. Cell Labeling with SPIO

rMSC-Fluc were cultured in DMEM supplemented with 2% FBS (Lonza; Basel, Switzerland), 1% MEM essential vitamin mixture (Lonza), 1% Non essential aminoacids (Sigma-Aldrich; St Louis, MO, USA), 2% v/v penicillin–streptomycin, 2% v/v L-glutamine and 0.5% v/v glutamax (Invitrogen). Cells were grown at 80% confluency and incubated with a mixture of ferumoxide-protamine sulfate. Cells were labeled as previously described (34,35). Briefly, ferumoxides (Endorem, Guerbet S.A., Paris, France; hydrodynamic diameter of 120–180 nm) were diluted in serum free DMEM to a final concentration of 100 ug/ml; protamine sulfate was added to a final concentration of 5 ug/ml. After 5 min of intermitted shaking, the solution was added to the cells. Twenty-four hours later cells were washed three times with 10 U/ml heparinized PBS, harvested by trypsinization, put through a 40 μm cell-strainer and counted. Nonviable cells were obtained by repeated freeze/thawing and brief sonication of the injection solution. Inductively coupled plasma optical emission spectroscopy (Optima 4300DV, Perkin Elmer, Norwalk, CT, USA) was used to quantify the intracellular uptake of iron.

5.3. Viability Assessment of Labeled cells

To assess any potential effect of cell labeling on cell viability or proliferation, we labeled cells (wild type and expressing luciferase) with SPIO (triplicate samples), harvested cells on different days, and counted the number of cells on an automatic cell counter. Doubling time was estimated assuming a exponential growth model: $A_t = A_0 2^{t/td}$ (where A_t is the cell number at time t; A_0 is the cell number at time 0; t is time; t_d is the doubling time) (36).

5.4. Cell Transplantation and *In Vivo* Imaging

All animal experiments were conducted in compliance with the independent Institutional Animal Welfare Committee. For assessing the reproducibility of R_2 mapping by MR imaging techniques, rats (Wistar; Harlan, Horst, the Netherlands; $n = 4$) underwent anesthesia and MRI for a total of four sessions each (on different days). Image analysis was performed by the same investigator who was blinded to the animal group and the previous evaluations. For experiments regarding tracking of implanted cells by MRI, rats (Wistar; Harlan, Horst, the Netherlands) received intramyocardial injections. Briefly, animals were induced with a 2% isoflurane (Baxter Healthcare, Deerfield, IL, USA)/oxygen mixture, and kept under anesthesia by the intraperitoneal administration of a combination of fentanyl (300 ug/kg) and medetomidine (300 ug/kg). Animals were orotracheally intubated and ventilated and left thoracotomy performed. After intramyocardial injection, the chest was closed, pneumothorax reduced and buprenorfine (0.1 mg/kg) administered subcutaneously. Group 1 ($n = 9$) received

1.5×10^6 viable rMSC SPIO-labeled cells; group 2 ($n = 5$) received 1.5×10^6 nonviable SPIO-labeled cells; group 3 ($n = 3$) received PBS injection (sham experiment). We allowed the animals to recover from surgery (cell implantation) and performed bioluminescence and MR at each time point.

5.5. Bioluminescence Studies

Optical bioluminescence was performed by using the charged coupled camera device Xenogen IVIS Spectrum (Caliper Life Sciences, Hopkington, MA, USA), 5 min after intraperitoneal administration of 150 mg/kg of D-luciferine (Promega). Each rat was imaged up to 30 min (integration time, 30, 60, 120, 180 s; f/stop, 1; binning, medium; field of view, B) to follow the pharmacokinetic profile of luciferin activation. Optical intensity was quantified in units of photons/second/cm^2/steradian. Regions of interest were used to calculate the optical peak value at the level of the implanted cells in the heart. Data were analyzed with the software Living Image 2.6 (Caliper LS, Perkin Elmer).

5.6. Magnetic Resonance Imaging

MRI data were acquired by using a 7 T scanner (Agilent-GE Discovery MR901 scanner, Milwaukee, WI, USA) with 300 mT/m max gradient. A 150 mm diameter quadrature coil was used for transmitting and a 4 channel Rx surface coil array for receiving the signal (Rapid Biomedical. Würzburg, Germany). Every exam started with routine cine sequences (two-chamber view and four-chamber view) to allow the proper positioning on the heart axial plane and the selection of the most representative section. The overall time required for slice positioning and scanning was 20 min.

Single cardiac phase with cardiac triggered double inversion BBFSE images were acquired on the short axis of the heart (18). The effective echo times of the separate scans were: $TE = 4.4$, 8.8, 13.2, 17.6, 22, 26.4 ms; $TR = 600$ ms. Image resolution was: field of view $= 50 \times 50$ mm; matrix $= 256 \times 256$, leading to an in-plane voxel size of 0.2×0.2 mm. Slice thickness was 1.8 mm. The scan time for all *TE* images was ~5 min. The triggering was provided by peripheral pulse oxygenation level monitoring on the hind leg of the rats (SA Instruments, Stony Brook, NY, USA). The echo train length was 6; the echo spacing was 4.4 ms, optimized to achieve the required span of available *TE* values, yet making sure that the echo train did not extend beyond the cardiac resting phase.

5.7. Image Processing

For reproducibility experiments, the inner and outer boundary of the myocardium were manually drawn on the short axis image with the shortest *TE*, with the highest signal-to-noise ratio. To correct for motion artifacts the image set was registered to the images with the shortest *TE* using a two-step approach. Five anatomical landmarks of the myocardium were manually selected to enable a point-based rigid registration, which was used as an initialization for an intensity-based mutual information-based rigid registration. The myocardium region was divided into standard sectors (37) and the six mid-ventricular regions were considered. The mean T_2 and the standard deviation were calculated for each region and each day.

For the quantification of SPIO-labeled rMSC, a region-of-interest was manually drawn on the short axis image at the level of the signal void (site of injection).

A T_2 map was then generated using a maximum likelihood estimator approach which takes the Rician noise distribution of the magnitude MR images into account (38). This maximum likelihood formulation also yields the Cramer–Rao lower bounds on the precision of the fits. The square root of the Cramer–Rao lower bounds is a lower bound on the standard deviation of the T_2 and can therefore be used as an error estimate in milliseconds.

5.8. Histology

For histological evaluation, hearts were harvested at 3 (one animal), 15 (four animals) and 28 (two animals, data not shown) days after injection, washed in ice-cold PBS, and fixed for 24 h in 4% paraformaldehyde, embedded in Tissue-TEK OCT compound (Sakura, Finetek U.S.A Inc.), frozen at −80 °C, and cryosectioned to obtain 10 μm-thick samples. Slides were stained for iron by using the Accustain kit (Iron stain; Sigma-Aldrich) and imaged by light microscopy.

5.9. Statistics

Statistical data were evaluated using Graphpad Prism 5.0 (Graphpad Software). Statistical comparisons between two experimental groups were performed using *t*-tests (unpaired comparisons); comparison of multiple groups was performed with two-way ANOVA using Bonferroni's multiple comparison *post hoc* analysis. Correlation analysis for nonparametric data was performed.

In the reproducibility experiments, intraclass correlation coefficients were performed to to estimate intraobserver variability for every region across animals (39); for every region the anaysis of variance has been calculated according to Levene's test followed by one-way ANOVA. All statistical comparisons were two-sided, and the level of statistical significance was set at $p < 0.05$. Unless differently specified, all values were reported as means ± standard error of the mean.

Acknowledgments

The authors thank Mr R. C. Janssens (Cell Biology, Erasmus MC, Rotterdam, The Netherlands) for technical assistance with the bioluminescence reporter gene, and Professor B Wolterbeek (Technical University Delft, Delft, The Netherlands) for assistance with the inductively coupled plasma optical emission spectroscopy measurements. This work wassupported in part by ENCITE European Network for Cell Imaging and Tracking Expertise (funded by the European Community under the 7th Framework program).

REFERENCES

1. Orlic D, Kajstura J, Chimenti S, Jakoniuk I, Anderson SM, Li B, Pickel J, McKay R, Nadal-Ginard B, Bodine DM, Leri A, Anversa P. Bone marrow cells regenerate infarcted myocardium. Nature 2001; 410 (6829): 701–705.
2. Lipinski MJ, Biondi-Zoccai GG, Abbate A, Khianey R, Sheiban I, Bartunek J, Vanderheyden M, Kim HS, Kang HJ, Strauer BE, Vetrovec GW. Impact of intracoronary cell therapy on left ventricular function in the setting of acute myocardial infarction: a collaborative systematic review and meta-analysis of controlled clinical trials. J Am Coll Cardiol 2007; 50(18): 1761–1767.
3. Martin-Rendon E, Brunskill SJ, Hyde CJ, Stanworth SJ, Mathur A, Watt SM. Autologous bone marrow stem cells to treat acute myocardial infarction: a systematic review. Eur Heart J 2008; 29(15): 1807–1818.
4. Korf-Klingebiel M, Kempf T, Sauer T, Brinkmann E, Fischer P, Meyer GP, Ganser A, Drexler H, Wollert KC. Bone marrow cells are a rich

source of growth factors and cytokines: implications for cell therapy trials after myocardial infarction. Eur Heart J 2008; 29(23): 2851–2858.
5. Ruggiero A, Thorek DL, Guenoun J, Krestin GP, Bernsen MR. Cell tracking in cardiac repair: what to image and how to image. Eur Radiol 2012; 22(1): 189–204.
6. Bernsen MR, Moelker AD, Wielopolski PA, van Tiel ST, Krestin GP. Labelling of mammalian cells for visualisation by MRI. Eur Radiol 20(2): 255–274.
7. Arbab AS, Pandit SD, Anderson SA, Yocum GT, Bur M, Frenkel V, Khuu HM, Read EJ, Frank JA. Magnetic resonance imaging and confocal microscopy studies of magnetically labeled endothelial progenitor cells trafficking to sites of tumor angiogenesis. Stem Cells 2006; 24(3): 671–678.
8. Delcroix GJ, Jacquart M, Lemaire L, Sindji L, Franconi F, Le Jeune JJ, Montero-Menei CN. Mesenchymal and neural stem cells labeled with HEDP-coated SPIO nanoparticles: in vitro characterization and migration potential in rat brain. Brain Res 2009; 1255: 18–31.
9. Farrell E, Wielopolski P, Pavljasevic P, Kops N, Weinans H, Bernsen MR, van Osch GJ. Cell labelling with superparamagnetic iron oxide has no effect on chondrocyte behaviour. Osteoarthritis Cartilage 2009; 17(7): 961–967.
10. van Tiel ST, Wielopolski PA, Houston GC, Krestin GP, Bernsen MR. Variations in labeling protocol influence incorporation, distribution and retention of iron oxide nanoparticles into human umbilical vein endothelial cells. Contrast Media Mol Imag 2010; 5(5): 247–257.
11. Amsalem Y, Mardor Y, Feinberg MS, Landa N, Miller L, Daniels D, Ocherashvilli A, Holbova R, Yosef O, Barbash IM, Leor J. Iron-oxide labeling and outcome of transplanted mesenchymal stem cells in the infarcted myocardium. Circulation 2007; 116(11 suppl): I38–45.
12. Winter EM, Hogers B, van der Graaf LM, Gittenberger-de Groot AC, Poelmann RE, van der Weerd L. Cell tracking using iron oxide fails to distinguish dead from living transplanted cells in the infarcted heart. Magn Reson Med 63(3): 817–821.
13. Kotek G, van Tiel ST, Wielopolski PA, Houston GC, Krestin GP, Bernsen MR. Cell quantification: evolution of compartmentalization and distribution of iron-oxide particles and labeled cells. Contrast Media Mol Imag 2012; 7(2): 195–203.
14. Kuhlpeter R, Dahnke H, Matuszewski L, Persigehl T, von Wallbrunn A, Allkemper T, Heindel WL, Schaeffter T, Bremer C. R_2 and R_2* mapping for sensing cell-bound superparamagnetic nanoparticles: in vitro and murine in vivo testing. Radiology 2007; 245(2): 449–457.
15. Simon GH, Bauer J, Saborovski O, Fu Y, Corot C, Wendland MF, Daldrup-Link HE. T1 and T2 relaxivity of intracellular and extracellular USPIO at 1.5T and 3T clinical MR scanning. Eur Radiol 2006; 16(3): 738–745.
16. Henning TD, Wendland MF, Golovko D, Sutton EJ, Sennino B, Malek F, Bauer JS, McDonald DM, Daldrup-Link H. Relaxation effects of ferucarbotran-labeled mesenchymal stem cells at 1.5T and 3T: discrimination of viable from lysed cells. Magn Reson Med 2009; 62(2): 325–332.
17. Rad AM, Arbab AS, Iskander AS, Jiang Q, Soltanian-Zadeh H. Quantification of superparamagnetic iron oxide (SPIO)-labeled cells using MRI. J Magn Reson Imag 2007; 26(2): 366–374.
18. Simonetti OP, Finn JP, White RD, Laub G, Henry DA. 'Black blood' T2-weighted inversion-recovery MR imaging of the heart. Radiology 1996; 199(1): 49–57.
19. Karamitsos TD, Francis JM, Myerson S, Selvanayagam JB, Neubauer S. The role of cardiovascular magnetic resonance imaging in heart failure. J Am Coll Cardiol 2009; 54(15): 1407–1424.
20. Chen IY, Wu JC. Cardiovascular molecular imaging: focus on clinical translation. Circulation 2011; 123(4): 425–443.
21. Giri S, Chung YC, Merchant A, Mihai G, Rajagopalan S, Raman SV, Simonetti OP. T2 quantification for improved detection of myocardial edema. J Cardiovasc Magn Reson 2009; 11: 56.
22. Aletras AH, Kellman P, Derbyshire JA, Arai AE. ACUT2E TSE-SSFP: a hybrid method for T2-weighted imaging of edema in the heart. Magn Reson Med 2008; 59(2): 229–235.
23. Payne AR, Casey M, McClure J, McGeoch R, Murphy A, Woodward R, Saul A, Bi X, Zuehlsdorff S, Oldroyd KG, Tzemos N, Berry C. Bright-blood T2-weighted MRI has higher diagnostic accuracy than dark-blood short tau inversion recovery MRI for detection of acute myocardial infarction and for assessment of the ischemic area at risk and myocardial salvage. Circ Cardiovasc Imag 2011; 4(3): 210–219.
24. Cocker MS, Shea SM, Strohm O, Green J, Abdel-Aty H, Friedrich MG. A new approach towards improved visualization of myocardial edema using T2-weighted imaging: a cardiovascular magnetic resonance (CMR) study. J Magn Reson Imag 2011; 34(2): 286–292.
25. Boutry S, Forge D, Burtea C, Mahieu I, Murariu O, Laurent S, Vander Elst L, Muller RN. How to quantify iron in an aqueous or biological matrix: a technical note. Contrast Media Mol Imag 2009; 4(6): 299–304.
26. Peldschus K, Schultze A, Nollau P, Kaul M, Schumacher U, Wagener C, Adam G, Ittrich H. Quantitative MR imaging of targeted SPIO particles on the cell surface and comparison to flow cytometry. Magn Reson Imag 2010; 28(4): 599–606.
27. Atalay MK, Poncelet BP, Kantor HL, Brady TJ, Weisskoff RM. Cardiac susceptibility artifacts arising from the heart-lung interface. Magn Reson Med 2001; 45(2): 341–345.
28. Chen IY, Greve JM, Gheysens O, Willmann JK, Rodriguez-Porcel M, Chu P, Sheikh AY, Faranesh AZ, Paulmurugan R, Yang PC, Wu JC, Gambhir SS. Comparison of optical bioluminescence reporter gene and superparamagnetic iron oxide MR contrast agent as cell markers for noninvasive imaging of cardiac cell transplantation. Mol Imag Biol 2009; 11(3): 178–187.
29. Muller-Ehmsen J, Whittaker P, Kloner RA, Dow JS, Sakoda T, Long TI, Laird PW, Kedes L. Survival and development of neonatal rat cardiomyocytes transplanted into adult myocardium. J Mol Cell Cardiol 2002; 34(2): 107–116.
30. Nakamura Y, Yasuda T, Weisel RD, Li RK. Enhanced cell transplantation: preventing apoptosis increases cell survival and ventricular function. Am J Physiol Heart Circul Physiol 2006; 291(2): H939–947.
31. Krishnan M, Park JM, Cao F, Wang D, Paulmurugan R, Tseng JR, Gonzalgo ML, Gambhir SS, Wu JC. Effects of epigenetic modulation on reporter gene expression: implications for stem cell imaging. FASEB J 2006; 20(1): 106–108.
32. Guenoun J, Ruggiero A, Doeswijk G, Janssens RC, Koning GA, Kotek G, Krestin GP, Bernsen MR. In vivo quantitative assessment of cell viability of gadolinium or iron-labeled cells using MRI and bioluminescence imaging. Contrast Media Mol Imag 2013; 8(2): 165–174.
33. Nedopil A, Klenk C, Kim C, Liu S, Wendland M, Golovko D, Schuster T, Sennino B, McDonald DM, Daldrup-Link HE. MR signal characteristics of viable and apoptotic human mesenchymal stem cells in matrix-associated stem cell implants for treatment of osteoarthritis. Invest Radiol 2010; 45(10): 634–640.
34. van Buul GM, Farrell E, Kops N, van Tiel ST, Bos PK, Weinans H, Krestin GP, van Osch GJ, Bernsen MR. Ferumoxides-protamine sulfate is more effective than ferucarbotran for cell labeling: implications for clinically applicable cell tracking using MRI. Contrast Media Mol Imag 2009; 4(5): 230–236.
35. van Buul GM, Kotek G, Wielopolski PA, Farrell E, Bos PK, Weinans H, Grohnert AU, Jahr H, Verhaar JA, Krestin GP, van Osch GJ, Bernsen MR. Clinically translatable cell tracking and quantification by MRI in cartilage repair using superparamagnetic iron oxides. PLoS One 2011; 6(2): e17001.
36. Roth V. http://www.doubling-time.com/compute.php, 2006.
37. Cerqueira MD, Weissman NJ, Dilsizian V, Jacobs AK, Kaul S, Laskey WK, Pennell DJ, Rumberger JA, Ryan T, Verani MS. Standardized myocardial segmentation and nomenclature for tomographic imaging of the heart: a statement for healthcare professionals from the Cardiac Imaging Committee of the Council on Clinical Cardiology of the American Heart Association. Circulation 2002; 105(4): 539–542.
38. Sijbers J, den Dekker AJ, Raman E, Van Dyck D. Parameter estimation from magnitude MR images. Int J Imag Syst Technol 1999; 10: 109–114.
39. Shrout PE, Fleiss JL. Intraclass correlations: uses in assessing rater reliability. Psychol Bull 1979; 86(2): 420–428.